UNIVERSITY
OF TRENTO

DIPARTIMENTO DI INGEGNERIA E SCIENZA DELL'INFORMAZIONE

38123 Povo – Trento (Italy), Via Sommarive 14
http://www.disi.unitn.it

MULTI-RESOLUTION ITERATIVE INVERSION OF REAL INHOMOGENEOUS TARGETS

M. Donelli, D. Franceschini, A. Massa, M. Pastorino, and A. Zanetti

December 2005

Technical Report # DISI-11-083

Multi-Resolution Iterative Inversion of Real Inhomogeneous Targets

M. Donelli,* D. Franceschini,* A. Massa,* M. Pastorino,** and A. Zanetti*

* Department of Information and Communication Technology

University of Trento -Via Sommarive, 14 - 38050 Trento - ITALY

Tel.: +39 0461 882057; Fax: +39 0461 882093

E-mail: *andrea.massa@ing.unitn.it*, {*massimo.donelli, davide.franceschini*}*@dit.unitn.it*

Web-site: *http://www.eledia.ing.unitn.it*

** Department of Biophysical and Electronic Engineering

University of Genoa -Via Opera Pia, 11A - 16145 Genova - ITALY

Tel.: +39 010 3532242; Fax: +39 010 3532245

E-mail: *pastorino@dibe.unige.it*

Multi-Resolution Iterative Inversion of Real Inhomogeneous Targets

M. Donelli, D. Franceschini, A. Massa, M. Pastorino, and A. Zanetti

Abstract

This paper presents a review of the reconstruction results obtained from the inversion of experimental data provided by the *Institute Fresnel* in Marseille (France) and concerned with inhomogeneous dielectric targets and hybrid configurations, where dielectric and metallic cylinders are present in the scenario under test. The Iterative Multi-Scaling Approach (IMSA) is applied for addressing the inversion of scattering data in order to effectively exploit the available information through a multi-step reconstruction procedure, which adaptively allocates a set of unknown coefficients, related to the dielectric distribution in the investigation area, on the basis of the information collected during the iterative process. The obtained results confirm the effectiveness of such an iterative multi-resolution strategy in dealing with complex scatterers already demonstrated in synthetic experiments.

1 Introduction and Inversion Strategy

The challenging issue of reconstructing unknown targets in inaccessible areas needs the development of more and more efficient and reliable inversion algorithms to be employed in several applied sciences. In this context, the availability of experimental data (e.g., [1]) is of great interest for testing the inversion methods since the reconstructions yielded from synthetically-generated data cannot represent an exhaustive test case because of the difficulties in representing the acquisition process as well as the unavoidable data corruption arising in real experiments. Furthermore, the use of real data prevents the inverse crime [2] occurring when the forward solver, which generates the scattering data, is closely related to the numerical code used in the inversion process.

In the framework of the experimental validation of inverse scattering techniques, the new database provided by the *Institute Fresnel* represents a novel and very challenging benchmark for testing the Iterative Multi-Scaling Approach [3]. Such a multi-resolution strategy has been so far employed in dealing with several synthetic and real configurations related to both single and multiple cylindrical structures [4][5], but never in reconstructing complex configurations as those considered in this database.

In order to properly comment the reconstruction experiments, let us briefly recall the key procedural steps of the IMSA. By referring to TM illumination conditions and omitting the time-factor $exp(j2\pi f)$ (f being the working frequency), the target is supposed to be illuminated by a finite set ($v = 1, ..., V$) of incident electromagnetic fields polarized along the vertical direction of the scatterer ($\underline{E}^v_{inc} = E^v_{inc}(x, y)\hat{\mathbf{z}};\ v = 1, ..., V$). The scattered electric field $\underline{E}^v_{scatt} = E^v_{scatt}\hat{\mathbf{z}}$ is collected at M measurement points located in an "observation domain" D_O external to the "investigation domain" D_I where the unknown scatterer is supposed to be located ($(x_{m_{(v)}}, y_{m_{(v)}}) \in D_O$, $m_{(v)} = 1, ..., M_{(v)}$, $v = 1, ..., V$).

The inversion problem consists in retrieving the distribution of the object function

$$\tau(x, y) = \varepsilon_r(x, y) - 1 - j\frac{\sigma(x, y)}{2\pi f \varepsilon_0}, \tag{1}$$

related to the dielectric permittivity $\varepsilon_r(x,y)$ and conductivity $\sigma(x,y)$ of the scatterer, in D_I by assuming a lossless non-magnetic background medium characterized by a dielectric permittivity ε_0. Towards this end, the scattering problem is mathematically described in terms of the well-known integral scattering equations [2]

$$E^v_{scatt}(x_{m(v)}, y_{m(v)}) = -k_0^2 \int_{D_I} G_{2d}(x_{m(v)}, y_{m(v)}|x', y')\tau(x', y')E^v_{tot}(x', y')dx'dy', \quad m_{(v)} = 1, ..., M_{(v)}$$
$$(x_{m_{(v)}},\, y_{m_{(v)}}) \in D_O \qquad v = 1, ..., V \tag{2}$$

(*Data Equation*)

$$E^v_{inc}(x,y) = E^v_{tot}(x,y) + k_0^2 \int_{D_I} G_{2d}(x,y|x',y')\tau(x',y')E^v_{tot}(x',y')dx'dy' \;\; (x,\, y) \in D_I \tag{3}$$

(*State Equation*)

(where G_{2d} and k_0 denote the Green's function [6] and the wavenumber of the background medium, respectively) and successively solved, after discretization [7], by means of the IMSA.

Summarizing, the Iterative Multi-Scaling Approach belongs to the class of multi-resolution algorithms (e.g., [8] and [9]), which consider a non-uniform discretization of D_I to achieve the optimal trade-off between the achievable spatial resolution accuracy and the limited amount of information collectable during the data acquisition [10]. According to an iterative strategy, the unknown scatterers are reconstructed through a multi-step ($s = 1, ..., S_{opt}$, s being the step index) process able to enhance the spatial resolution in a set of regions-of-interest (RoIs) where the objects have been localized [5]. The resolution level is increased without enlarging the space of the unknowns and keeping a constant ratio between data and unknowns that favorably affects the false solutions problem. Moreover, adapting the number of unknowns during the multistep process is somehow an intrinsic regularization because the iteration searches for a finite dimensional image subspace. The multiresolution strategy is mathematically implemented by defining at each step s of the

multi-scaling process the multi-resolution cost function[1] that involves the discretized versions of integral relations (2)(3)

$$\Phi^{(s)}\left\{\tau^{(s)}\left(x_{n_{(r)}},y_{n_{(r)}}\right),\ E_{tot}^{v\,(s)}\left(x_{n_{(r)}},y_{n_{(r)}}\right);\ \begin{array}{rr} r=1,...,R=s; \\ n_{(r)}=1,...,N_{(r)}; \quad v=1,...,V \end{array}\right\}= \quad (4)$$

$$\frac{\sum_{v=1}^{V}\sum_{m=1}^{M}\left|E_{scatt}^{v}(x_m,y_m)-\Omega_{ext}^{m,v}\right|^2}{\sum_{v=1}^{V}\sum_{m=1}^{M}\left|E_{scatt}^{v}(x_m,y_m)\right|^2}$$

$$+\frac{\sum_{v=1}^{V}\sum_{r=1}^{R}\sum_{n_{(r)}=1}^{N_{(r)}}\left\{w\left(x_{n_{(r)}},y_{n_{(r)}}\right)\left|E_{inc}^{v}\left(x_{n_{(r)}},y_{n_{(r)}}\right)-\Omega_{int}^{n_{(r)},v}\right|\right\}^2}{\sum_{v=1}^{V}\sum_{r=1}^{R}\sum_{n_{(r)}=1}^{N_{(r)}}\left\{w\left(x_{n_{(r)}},y_{n_{(r)}}\right)\left|E_{inc}^{v}\left(x_{n_{(r)}},y_{n_{(r)}}\right)\right|\right\}^2}$$

where

$$\Omega_{ext}^{m,v}=\sum_{r=1}^{R}\sum_{n_{(r)}=1}^{N_{(r)}}\left\{w\left(x_{n_{(r)}},y_{n_{(r)}}\right)\tau^{(s)}\left(x_{n_{(r)}},y_{n_{(r)}}\right)E_{tot}^{v\,(s)}\left(x_{n_{(r)}},y_{n_{(r)}}\right)G_{2d}^{ext}\left(A_{n_{(r)}},\rho_{n_{(r)}m}\right)\right\} \quad (5)$$

$$\Omega_{int}^{n_{(r)},v}=E_{tot}^{v\,(s)}\left(x_{n_{(r)}},y_{n_{(r)}}\right)-\sum_{u_{(r)}=1}^{N_{(r)}}\left\{\tau^{(s)}\left(x_{u_{(r)}},y_{u_{(r)}}\right)E_{tot}^{v\,(s)}\left(x_{u_{(r)}},y_{u_{(r)}}\right)G_{2d}^{int}\left(A_{u_{(r)}},\rho_{u_{(r)}n_{(r)}}\right)\right\} \quad (6)$$

and $G_{2d}^{ext}\left(A_{n_{(r)}},\rho_{n_{(r)}m}\right)$ and $G_{2d}^{int}\left(A_{u_{(r)}},\rho_{u_{(r)}n_{(r)}}\right)$ indicate the discretized forms of the Green integrals [3]; $\rho_{n_{(r)}m}=\sqrt{\left(x_{n_{(r)}}-x_m\right)^2+\left(y_{n_{(r)}}-y_m\right)^2}$; $\rho_{u_{(r)}n_{(r)}}=\sqrt{\left(x_{u_{(r)}}-x_{n_{(r)}}\right)^2+\left(y_{u_{(r)}}-y_{n_{(r)}}\right)^2}$; $A_{n_{(r)}}\left(or\ A_{u_{(r)}}\right)=l_{(r)}^2$ is the area of the n-th cell (or u-th cell) at the r-th resolution level. Moreover, the w is the weighting function defined as follows

$$w(x_{n_{(r)}},y_{n_{(r)}})=\begin{cases}0 & if\ \ (x_{n_{(r)}},y_{n_{(r)}})\notin D_{RoI(s-1)}\\ 1 & if\ \ (x_{n_{(r)}},y_{n_{(r)}})\in D_{RoI(s-1)}\end{cases} \quad (7)$$

and updated at the beginning of each minimization step (s) according to the support of the RoI ($D_{RoI(s-1)}$) defined at the end of the (s-*1*)-th step. Such RoI is a squared area

[1] For compactness and simplicity, let us set $m_{(v)}=m$ and $M_{(v)}=M$ for $v=1,...,V$.

centered at

$$x_{c_{(s-1)}} = \frac{x_{re_{(s-1)}} + x_{im_{(s-1)}}}{2}, \quad y_{c_{(s-1)}} = \frac{y_{re_{(s-1)}} + y_{im_{(s-1)}}}{2} \tag{8}$$

$$x_{\Re(s-1)} = \frac{\sum_{r=1}^{R} \sum_{n_{(r)}=1}^{N_{(r)}} \left\{ x_{n_{(r)}} \Re\left[\tau^{(s-1)}\left(x_{n_{(r)}}, y_{n_{(r)}} \right) \right] \right\}}{\sum_{n_{(r)}=1}^{N_{(r)}} \left\{ \Re\left[\tau^{(s-1)}\left(x_{n_{(r)}}, y_{n_{(r)}} \right) \right] \right\}}, \quad R = s-1 \tag{9}$$

$$y_{\Re(s-1)} = \frac{\sum_{r=1}^{R} \sum_{n_{(r)}=1}^{N_{(r)}} \left\{ y_{n_{(r)}} \Re\left[\tau^{(s-1)}\left(x_{n_{(r)}}, y_{n_{(r)}} \right) \right] \right\}}{\sum_{n_{(r)}=1}^{N_{(r)}} \left\{ \Re\left[\tau^{(s-1)}\left(x_{n_{(r)}}, y_{n_{(r)}} \right) \right] \right\}} \tag{10}$$

where $\Re$ stands for the real or the imaginary part. The side of such area ($L_{(s-1)}$) is determined after defining the RoIs of the real $\left(D^{Re}_{RoI(s-1)}\right)$ and of the imaginary part $\left(D^{Im}_{RoI(s-1)}\right)$ of the reconstructed profile. $\left(D^{Re}_{RoI(s-1)}\right)$ and $\left(D^{Im}_{RoI(s-1)}\right)$ are the regions whose side is given by the following expression

$$L_{\Re(s-1)} = 2 \frac{\sum_{r=1}^{R} \sum_{n_{(r)}=1}^{N_{(r)}} \left\{ \frac{\rho_{n_{(r)}\Re_{(s-1)}} \Re\left[\tau^{(s-1)}\left(x_{n_{(r)}}, y_{n_{(r)}} \right) \right]}{max_{n_{(r)}=1,..,N_{(r)}} \left\{ \Re\left[\tau^{(s-1)}\left(x_{n_{(r)}}, y_{n_{(r)}} \right) \right] \right\}} \right\}}{\sum_{r=1}^{R} \sum_{n_{(r)}=1}^{N_{(r)}} \left\{ \frac{\Re\left[\tau^{(s-1)}\left(x_{n_{(r)}}, y_{n_{(r)}} \right) \right]}{max_{n_{(r)}=1,..,N_{(r)}} \left\{ \Re\left[\tau^{(s-1)}\left(x_{n_{(r)}}, y_{n_{(r)}} \right) \right] \right\}} \right\}} \tag{11}$$

being $\rho_{n_{(r)}\Re_{(s-1)}} = \sqrt{\left(x_{n_{(r)}} - x_{\Re_{(s-1)}} \right)^2 + \left(y_{n_{(r)}} - y_{\Re_{(s-1)}} \right)^2}$. Consequently, the domain $D_{RoI(s-1)}$ is the minimum square area centered at $\left(x_{c_{(s-1)}}, y_{c_{(s-1)}} \right)$ that contains the region

$$\Omega_{(s-1)} = \left\{ D^{Re}_{RoI(s-1)} \cup D^{Im}_{RoI(s-1)} \right\} \tag{12}$$

Then, a noise filtering is performed in order to eliminate some artifacts in the reconstructed image. The new dielectric distribution turns out to be:

$$\widetilde{\tau}^{(s-1)}(x_{n_{(r)}}, y_{n_{(r)}}) = \begin{cases} \tau_0 & if \quad \begin{cases} \tau^{(s-1)}(x_{n_{(r)}}, y_{n_{(r)}}) < \tau_{th} \\ \left(x_{n_{(r)}}, y_{n_{(r)}}\right) \notin D_{(s-1)} \end{cases} \\ \dfrac{\sum_{j=1}^{J}\left\{\tau^{(s-1)}(x_j, y_j)\right\}}{J} & if \quad \begin{cases} \tau^{(s-1)}(x_{n_{(r)}}, y_{n_{(r)}}) \geq \tau_{th} \\ \left(x_{n_{(r)}}, y_{n_{(r)}}\right) \notin D_{(s-1)} \end{cases} \\ \tau^{(s-1)}(x_{n_{(r)}}, y_{n_{(r)}}) & elsewhere \end{cases} \tag{13}$$

where τ_{th} is a fixed threshold heuristically defined ($\tau_{th} = 0.2\, max_{n_{(r)}=1,..,N_{(r)}}\left\{\tau^{(s-1)}\left(x_{n_{(r)}}, y_{n_{(r)}}\right)\right\}$, $\left(x_{n_{(r)}}, y_{n_{(r)}}\right) \in D_{(s-1)}$) and τ_0 is the value of the contrast function for the background medium. Moreover, J is the dimension of the complete neighborhood system of the sub-domain located at $(x_{n_{(r)}}, y_{n_{(r)}})$ and (x_j, y_j) indicates a neighboring position.

Terminated the filtering procedure, at the successive step s of the iterative process, $\tau^{(s)}\left(x_{n_{(r)}}, y_{n_{(r)}}\right)$ and $E_{tot}^{v\,(s)}\left(x_{n_{(r)}}, y_{n_{(r)}}\right)$ are updated minimizing the cost function (4) by means of a conjugate gradient algorithm [3], but, in general, any available minimization tool could also be employed. The multi-step process is iteratively repeated until the stationarity criteria hold ($s = S_{opt}$) [5].

Since the knowledge of the incident field (i.e., the field without the scatterers) at different points $\left(x_{n_{(r)}}, y_{n_{(r)}}\right)$, $r = 1, ..., R$, in the investigation domain is needed to the IMSA to work properly and the "Marseille 2004" benchmark does not provide such an information (available only in D_O), the first problem to be faced in the numerical analysis is the modeling of the incident field. Towards this end, Sub-Section 2.1 addresses the issue of the numerical representation of the electromagnetic source. Starting from the obtained indications and guidelines, the effectiveness of the IMSA in reconstructing different configurations at various frequencies is assessed through a careful analysis of representative results. Finally, some comments on the feasibility and potentialities of the method in dealing with real data are reported (Sect. 3).

2 Reconstructions Results

In this Section, a selected set of results under TM conditions and concerned with four reference sets ("*FoamDielIntTM*", "*FoamDielExtTM*", "*FoamTwinDielTM*", and "*FoamMetExtTM*") provided by the *Institute Fresnel* in Marseille (France) are presented. The experimental setup as well as the database are described in the introduction to the special section and, in our experiments, a square investigation domain $\ell_{DI} = 30\,cm$ in side, has been chosen in order to limit the area where the unknown scatterers are supposed to lie (Fig. 1). As far as the *a-priori* information used in the reconstruction is concerned, the scatterers have been assumed to be lossless when dielectric configurations was considered ("*FoamDielIntTM*", "*FoamDielExtTM*", "*FoamTwinDielTM*"), while a "blind" inversion has been carried out for the hybrid configuration ("*FoamMetExtTM*") avoiding any a-priori assumption on the nature - dielectric or metallic - of the objects. Moreover, even though different datasets have been employed, always single-frequency measurements have been used for the reconstruction. Neither hopping nor multi-frequency strategies have been considered. Furthermore, no additional regularization terms in (4), edge-preserving methodologies or penalty terms have been taken into account in order to focus on the capabilities of the IMSA.

2.1 Model of the Incident Field

As previously pointed out, the IMSA needs the modeling of the incident field in the scattering domain D_I. Therefore, the first problem to be faced when adapting the multi-scaling approach to the experimental setup is related to the definition of a suitable model of the electromagnetic source, which allows a reasonable trade-off between simplicity and effectiveness in reproducing the samples of E^v_{inc} measured in D_O along the circular measurement line of radius 1.67 m.

As a preliminary step towards this end, a set of experiments has been performed in order to focus on the role of the knowledge of the incident field in the reconstruc-

tion process. Towards this aim, two datasets have been selected as cases-of-study: the "*FoamDielIntTM*" and the "*FoamDielExtTM*" datasets. In particular, the scattered data collected at $f = 4\,GHz$ have been processed taking into account the information about the incident field (supposed to be of plane wave type) only for determining the initial guess of the distribution of the total field inside the investigation domain. Consequently, the cost function (4) is only constituted by the "*Data Term*". Moreover, because of the aspect-limited nature of the experimental arrangement, all the available data ($M = 241$, $V = 8$) have been considered for reconstructing the unknown dielectric distribution in the investigation domain partitioned into $N = 16 \times 16$ square sub-domains at the initialization ($s = 1$) of the IMSA.

The reconstructed contrasts are shown in Figs. $2(a)$-$2(b)$ where the dashed lines superimposed to the gray-levels maps indicate the contours of the actual scatterers. The reconstructions are unsatisfactory since only the localizations of the supports of the scatterers are revealed, but the different regions of the inhomogeneous scatterers are not detected. Such indications clearly point out that the knowledge of the incident field cannot be neglected for providing reliable reconstructions.

Since the electromagnetic sources/sensors of the experimental setup are horn antennas and a detailed numerical model is not available (or it is not so-simple), the radiators are usually approximated with more simplified sources. In order to define the most suitable equivalent source, several simulations concerned with different models have been performed starting from the samples of the incident field measured in the observation curve.

Fig. 3 shows (in a restricted area $20\,cm$-sided) the retrieved profiles for the "*FoamDielIntTM*" and the "*FoamDielExtTM*" datasets when the incident field is modeled through a plane wave [Figs. $3(a)$-$3(b)$] or generated by a line source [Figs. $3(c)$-$3(d)$]. Quite accurate reconstructions can be observed when the plane-wave model is used. As far as the *"FoamDielIntTM"* test case is concerned [Fig. $3(a)$], two different regions can be distinguished. However, even though the peak value of the inner region is about $\tau_{max}^{int} = 2.02$ (i.e., very close to the actual one), the homogeneity of the outer region is not faithfully

reconstructed since the value of the object function turns out to be of about $\tau \approx 1.0$ (instead of $\tau = 0.45$) in many pixels. Similar conclusions hold true for the *"FoamDielExtTM"* scattering configuration [Fig. $3(b)$]. The results improve generating the incident field with the line current model [Figs. $3(c)$-(d)].

Moreover, a further improvement in the reconstruction accuracy has been obtained employing a *distributed-line-currents* (DLC) model. In this case, the actual source is replaced with a linear array of equally-spaced line-sources, which radiates an electric field given by

$$E_{inc}^{v}(x,\, y) = -\frac{k_0^2}{8\pi f \varepsilon_0} \sum_{p=1}^{P} A\,(x_p,\, y_p)\, H_0^{(2)}\,(k_0 \rho_p) \tag{14}$$

where $A(x_p,\, y_p)$ is an unknown parameter related to the *p-th* element to be calibrated, ρ_p the distance between the point where the field is computed and the *p-th* line source, and $H_0^{(2)}\,(k_0\rho_p)$ is the *0*-th order *2*-th kind Hankel function. As far as the calibration is concerned, whatever the working frequency f, the unknown coefficients $A(x_p,\, y_p)$ as well as P have been computed through the solution of an inverse-source problem where the known terms were the available samples of $E_{inc}^{v}(x_{m(v)}, y_{m(v)})$, $(x_{m_{(v)}},\, y_{m_{(v)}}) \in D_O$ provided by the experimental dataset.

Concerning the two configurations under test, the model has been synthesized with a linear array of $P = 15$ equally-spaced line currents positioned at $r_s = 1.67\, m$. P has been empirically determined selecting the number of line sources that are able to provide a good matching between the values of the incident field measured at the receivers and those computed by means of the numerical model. By considering such an approximation of the incident field, the dielectric profiles retrieved at the end of the multi-step process are displayed in Figs. $3(e)$-$3(f)$. As can be observed, both the qualitative and the quantitative imaging accuracy improve especially for the *"FoamDielExtTM"* configuration [Fig. $3(f)$]. More in detail, the scatterers are better shaped and the estimation of the dielectric parameters turns out to be better. As an example, for the *"FoamDielExtTM"* scenario, the value of τ of the weak scatterer is lower than $\tau_{max} = 0.6$.

Therefore, because of the better reconstruction performance with the DLC model obtained without increasing the computational cost, the inversion of experimental data has been carried out by using the model analytically described in (14).

2.2 Reconstruction Results

2.2.1 "*FomDielIntTM*" Dataset

The first set of reconstruction results is concerned with the configuration "*FomDielIntTM*" in the frequency range between $f = 2\,GHz$ and $f = 6\,GHz$. Pictorial representations of the reconstructed profiles at $s = S_{opt}$ of the multi-step process are shown in Fig. 4 when all the scattering data ($M = 241$ and $V = 8$) are used and $f = 2\,GHz$ [Fig. 4(a)], $f = 3\,GHz$ [Fig. 4(b)], $f = 5\,GHz$ [Fig. 4(c)] and $f = 6\,GHz$ [Fig. 4(d)]. Thus, the square investigation area, ℓ_{DI}-sided, ranges from $2\lambda_0 \times 2\lambda_0$ ($f = 2GHz$) to $6\lambda_0 \times 6\lambda_0$ ($f = 6GHz$). As can be noticed, whatever frequency in the range $f \in [2\,GHz, 6\,GHz]$, the layered structure of the actual object is clearly distinguishable. On the contrary, the quality of the reconstruction significantly decreases for higher frequencies since the IMSA turns out to be effective only in locating the scatterers without providing a faithful estimation of their dielectric properties.

As far as the dimension of the data-space is concerned, it should be pointed out that, from a theoretical point of view [10], a smaller number of samples is sufficient for collecting all the available information. In order to verify such a hypothesis, even though in an aspect-limited data situation, another experiment has been carried out by considering a reduced number of samples [12]. More in detail, the following configurations have been used: $M = 25$ - $V = 8$ ($f = 3\,GHz$) and $M = 41$ - $V = 8$ ($f = 5\,GHz$). The obtained results still remain accurate as can be observed comparing Figs. 4(e)-4(b) and Figs. 4(f)-4(c), respectively.

2.2.2 "*FoamDielExtTM*" Dataset

The second case-of-study is concerned with the *"FoamDielExtTM*" dataset where the scattered data are collected in presence of two different scatterers (both in dimension and dielectric characteristics) located the one close to the other. According to the previous results, the inversion problem has been performed considering the data in the range $f = 2 - 6\,GHz$ and a proper number of samples of the scattered field (Tab. I).

The quality of the estimated distributions turns out to be inadequate at the working frequency of $f = 2\,GHz$ [Fig. $5(a)$], $f = 3\,GHz$ [Fig. $5(b)$], and $f = 5\,GHz$ [Fig. $5(c)$], especially when compared to reconstruction yielded at $f = 6\,GHz$ [Fig. $5(d)$]. Such a behavior is probably caused by the limited number of data in presence of an environmental noise and errors in the modeling of the electromagnetic source. As a matter of fact, besides the limited-angle aspect of the data, many and unavoidable errors occur during the data-acquisition, which affect some measures. Therefore, a larger amount of data samples could positively influence the reconstruction by completing the collected information and concealing the errors. As expected, the use of the whole set of measures ($M = 241$, $V = 8$) allows a non-negligible enhancement in the reconstruction as shown in the representative samples of Figs. $5(e)$-$5(f)$.

Then, even though a reduced set of measurements has yielded to successful reconstructions in some experiments [e.g., Fig. $5(d)$], such a conclusion can not be drawn for all the analyzed datasets. Further studies should be pursued in order to understand if the choice of the subset of measurements that allows reliable reconstructions depend on the specific dataset and if considering a large number of data generally helps to prevent unsatisfactory inversions as those obtained in some experiments with the test case "*FoamDielExtTM*".

2.2.3 "*FoamTwinDielTM*" Dataset

As far as the "*FoamTwinDielTM*" dataset is concerned, the scattering data have been successfully processed in the range from $f = 2\,GHz$ up to $f = 4\,GHz$. The profiles retrieved

in correspondence with $M = 241$ scattered samples and $V = 18$ different illuminations are shown in Figs. $6(a)$-(c). Once again, the effectiveness of the IMSA in reconstructing inhomogeneous scatterers is confirmed.

2.2.4 "*FoamMetExtTM*" Dataset

The last example deals with the reconstruction of the hybrid configuration involving both dielectric and metallic scatterers. No *a-priori* information on the nature of the scatterers (metallic/dielectric) has been used during the inversion process and a "blind" reconstruction has been performed. Under such operating conditions, the best results in terms of retrieved distributions are shown in Figs. $7(a)$-$7(b)$ ($f = 4\,GHz$) and $7(c)$-$7(d)$ ($f = 6\,GHz$).

Notwithstanding the presence of some artifacts in the real part of the object function [Fig. $7(a)$ and Fig. $7(c)$], the retrieved images reveal that two objects lie in the investigation domain. The first one has been correctly imaged as a lossless scatterer [Fig. $7(a)$ and Fig. $7(c)$], while a metallic object can be identified in the gray-levels representation of $Im(\tau)$ [Fig. $7(b)$ and Fig. $7(d)$].

3 Conclusions

Thanks to the experimental benchmark provided by the *Institute Fresnel* and concerned with inhomogeneous and/or multiple targets, an exhaustive assessment of the capabilities and current limitations of the Iterative Multi-Scaling Approach against real data has been carried out. The inversion problem in hand has been successfully solved by approximating the electromagnetic source through a suitable distributed-line-currents model and according to a multi-step process. As far as the quality of the reconstructions is concerned, the approach has been able to correctly locate the supports of the scatterers as well as quantitatively image the unknown objects whatever the operating frequency, while faithful reconstructions, in terms of dielectric distributions (*quantitative imaging*), have

been generally achieved when $f \leq 6\,GHz$. Since the inversion method can be considered a "bare" approach, it is expected that the obtained performance will improve by properly adding the available *a-priori* information on the scatterers or by considering suitable edge-preserving strategies or frequency-hopping/multi-frequency procedures currently under development.

Acknowledgment

The authors wish to thank M. Saillard and K. Belkebir, Institute Fresnel, Marseille, France, for providing the experimental data and for the kind invitation to submit a contribution to the present special section.

References

[1] K. Belkebir and M. Saillard, Special section: "Testing Inversion Algorithms against Experimental Data," Inverse Problems, vol. 17, pp. 1565-1702, 2001.

[2] D. Colton and R. Kress, *Inverse Acoustic and Electromagnetic Scattering Theory.* New York: Springer, 1992.

[3] S. Caorsi, M. Donelli, D. Franceschini, and A. Massa, "A new methodology based on an iterative multi-scaling for microwave imaging," *IEEE Trans. Microwave Theory Tech.*, vol. 51, pp. 1162-1173, 2003.

[4] S. Caorsi, M. Donelli, and A. Massa, "Analysis of the stability and robustness of the iterative multi-scaling approach for microwave imaging applications," *Radioscience*, vol. 39, doi: 10.1029/2003RS002966, 2004.

[5] S. Caorsi, M. Donelli, and A. Massa, "Location, detection, and imaging of multiple scatterers by means of the iterative multiscaling method", *IEEE Trans. Microwave Theory Tech.*, vol. 52, pp. 1217-1228, 2004.

[6] D. Jones, *The Theory of Electromagnetism*. Oxford, U.K.: Pergamon Press, 1964.

[7] J. H. Richmond, "Scattering by a dielectric cylinder of arbitrary cross section shape," *IEEE Trans. Antennas Propagat.*, vol. 13, pp. 334-341, 1965.

[8] E. L. Miller and A. S. Willsky, "A multiscale, statistically based inversion scheme for linearized inverse scattering problems," *IEEE Trans. Geosci. Remote Sensing*, vol. 34, pp. 346-357, 1996.

[9] O. M. Bucci, L. Crocco, and T. Isernia, "An adaptive wavelet-based approach for non destructive evaluation applications," *Proc. Antennas and Propagation Symp.*, APS-2000, vol. 3, pp. 1756-1759.

[10] O. M. Bucci, and G. Franceschetti, "On the Degrees of Freedom of Scattered Fields," *IEEE Trans. on Ant. and Prop.,* vol. 37, pp. 918-926, 1989.

[11] R. E. Kleinman and P. M. Van den Berg, "A modified gradient method for two-dimensional problems in tomography," *J. Comput. Appl. Math.*, vol. 42, pp. 17-35, 1992.

[12] O. M. Bucci, and T. Isernia, Electromagnetic inverse scattering: retrievable information and measurements strategies, *Radio Science*, vol. 32, pp. 2123-2138, 1997.

Figure Captions

- **Figure 1.** Sketch of the imaging configuration and of the target region.

- **Figure 2.** Retrieved contrasts when $f = 4GHz$ for the datasets *"FoamDielIntTM"* (a) and *"FoamDielExtTM"* (b) neglecting the information on the incident field in D_I.

- **Figure 3.** Reconstruction results for the "*FoamDielIntTM*" $(a)(c)(e)$ and "*FoamDielExtTM*" $(b)(d)(f)$ datasets when the incident field is modeled through a plane wave model $[(a)(b)]$, a line source model $[(c)(d)]$, and a distributed line-current model $[(e)(f)]$.

- **Figure 4.** Reconstruction results for the "*FoamDielIntTM*" dataset at (a) $f = 2\,GHz$, (b) $f = 3\,GHz$, (c) $f = 5\,GHz$ (c), and (d) $f = 6\,GHz$ $(M = 241$ - $V = 8)$. Reconstruction results when (e) $M = 25$ - $V = 8$ $(f = 3\,GHz)$ and (f) $M = 41$ - $V = 8$ $(f = 5\,GHz)$.

- **Figure 5.** Reconstruction results for the "*FoamDielExtTM*" dataset when (a) $f = 2\,GHz$ $(M = 17$ - $V = 8)$, (b) $f = 3\,GHz$ $(M = 25$ - $V = 8)$, (c) $f = 5\,GHz$ $(M = 31$ - $V = 8)$, (d) $f = 6\,GHz$ $(M = 49$ - $V = 8)$. Samples of the retrieved profiles when $M = 241$ and $V = 8$: (e) $f = 2\,GHz$ and (f) $f = 5\,GHz$.

- **Figure 6.** Reconstruction results for the "*FoamTwinDielTM*" dataset $(M = 241$ - $V = 8)$: (a) $f = 2\,GHz$, (b) $f = 3\,GHz$, and (c) $f = 4\,GHz$.

- **Figure 7.** Reconstruction results for the "*FoamMetExtTM*" dataset at the working frequency of $f = 4GHz$ $[(a)$ real part and (b) imaginary part of the object function$]$ and $f = 6GHz$ $[(c)$ real part and (d) imaginary part of the object function$]$.

Table Captions

- **Table I.** Parameters used for the inversion of the "*FoamDielExtTM*" dataset.

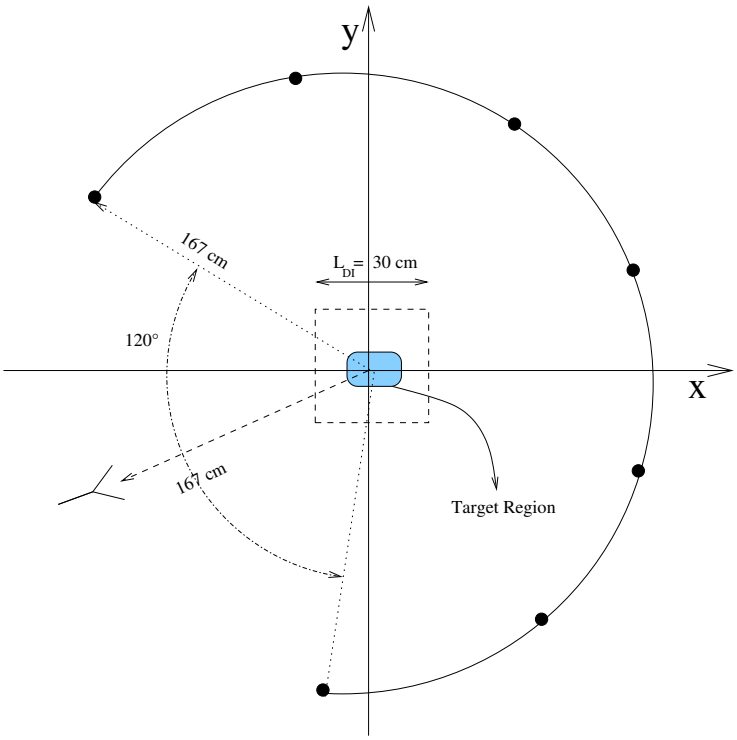

Figure 1 - M. Donelli *et al.*, "*Multi-Resolution Iterative....*"

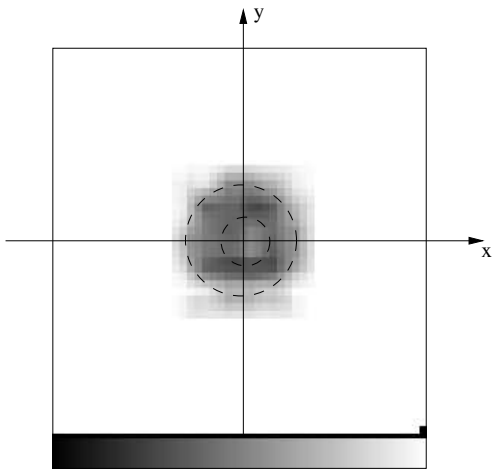

2.6 $Re\{\tau(x,y)\}$ 0.0

(a)

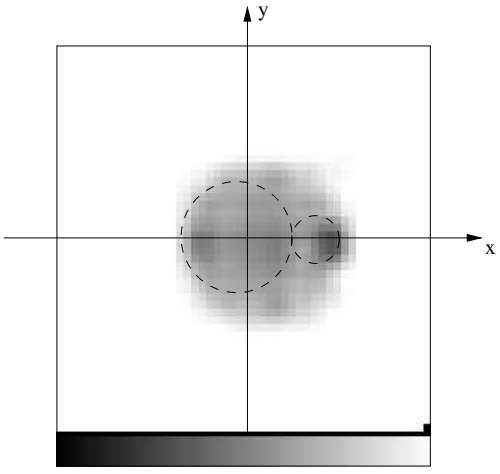

2.6 $Re\{\tau(x,y)\}$ 0.0

(b)

Figure 2 - M. Donelli *et al.*, "*Multi-Resolution Iterative....*"

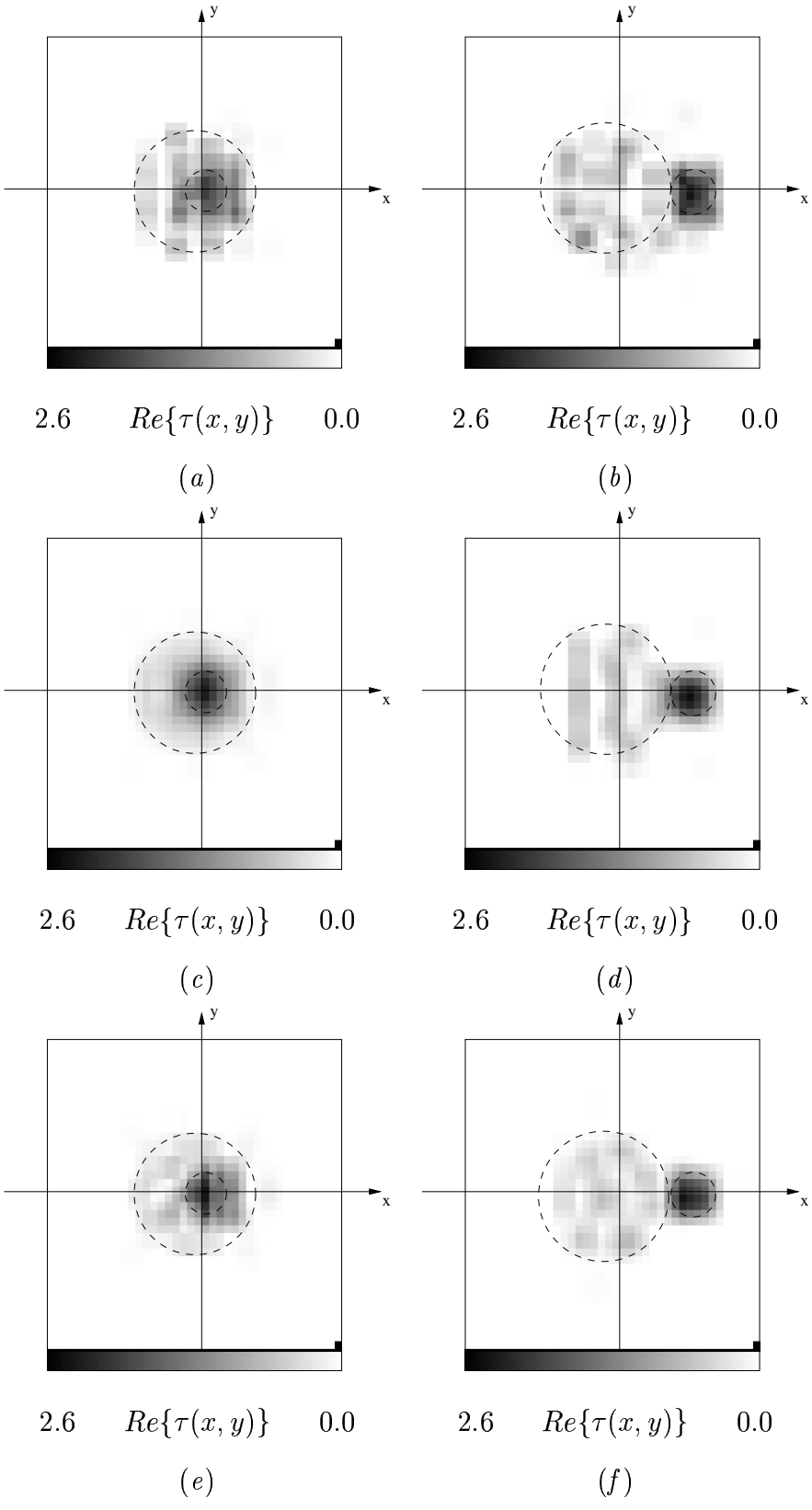

Figure 3 - M. Donelli *et al.*, "*Multi-Resolution Iterative....*"

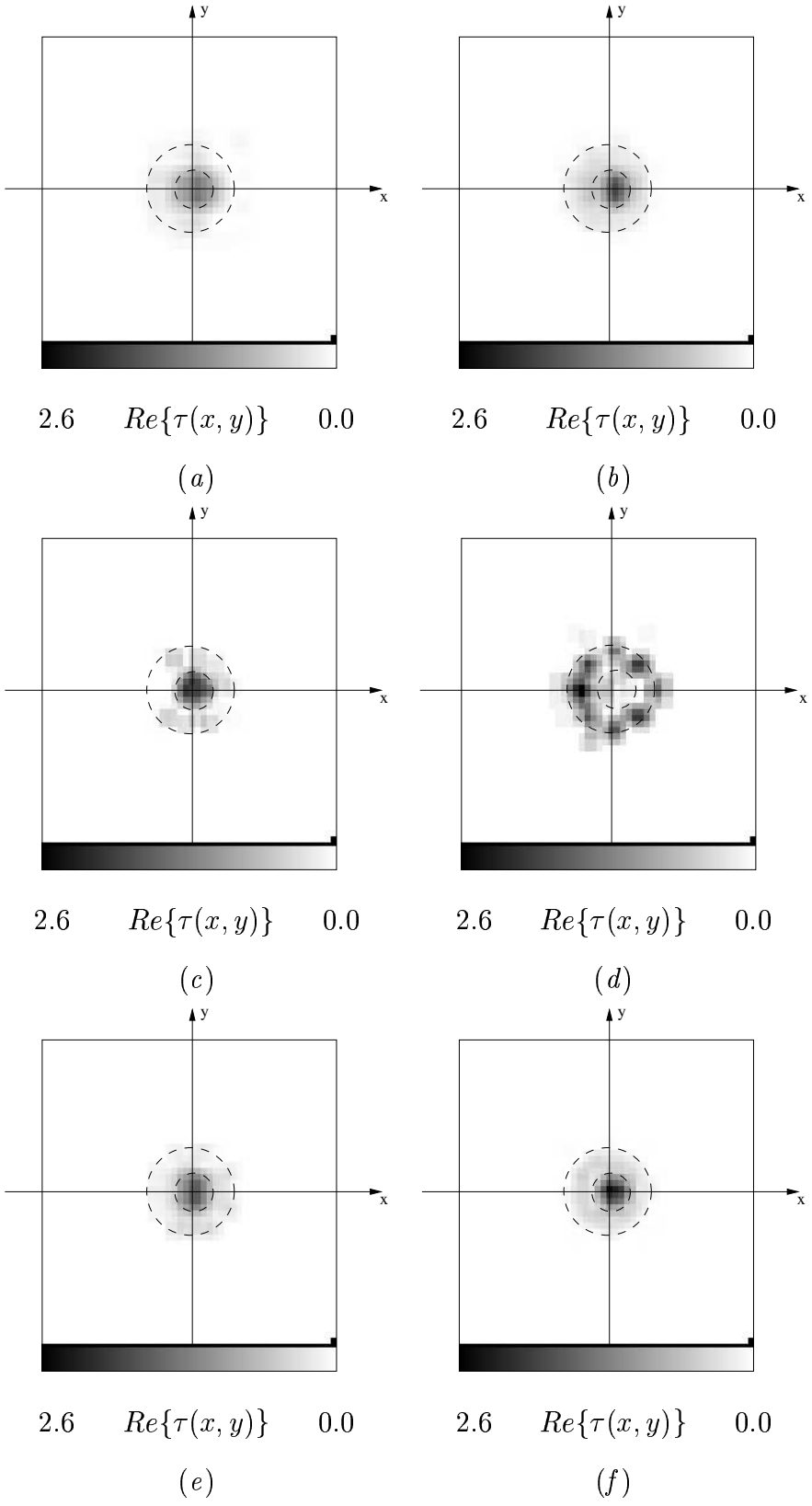

Figure 4 - M. Donelli *et al.*, "*Multi-Resolution Iterative....*"

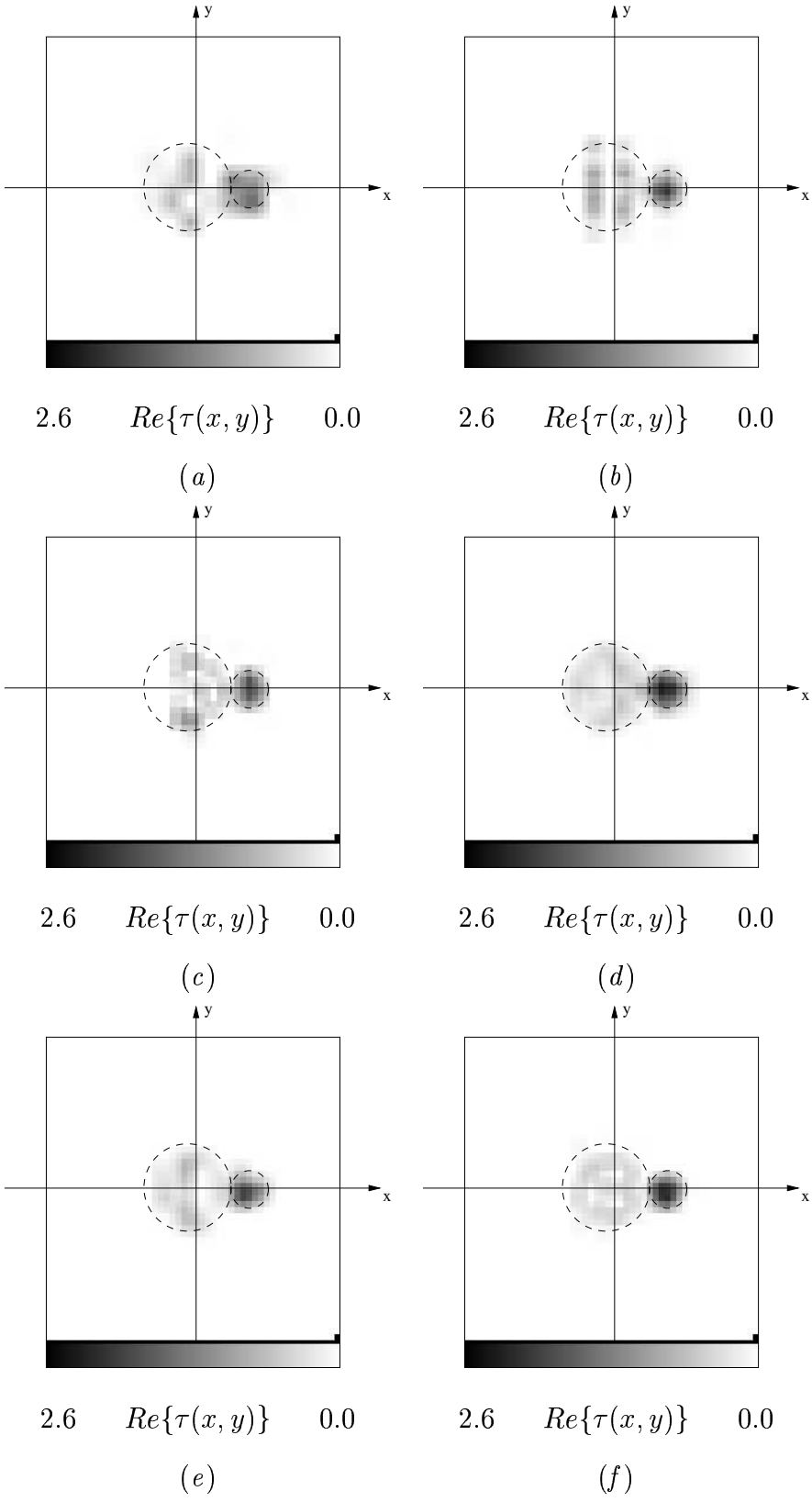

Figure 5 - M. Donelli *et al.*, "*Multi-Resolution Iterative....*"

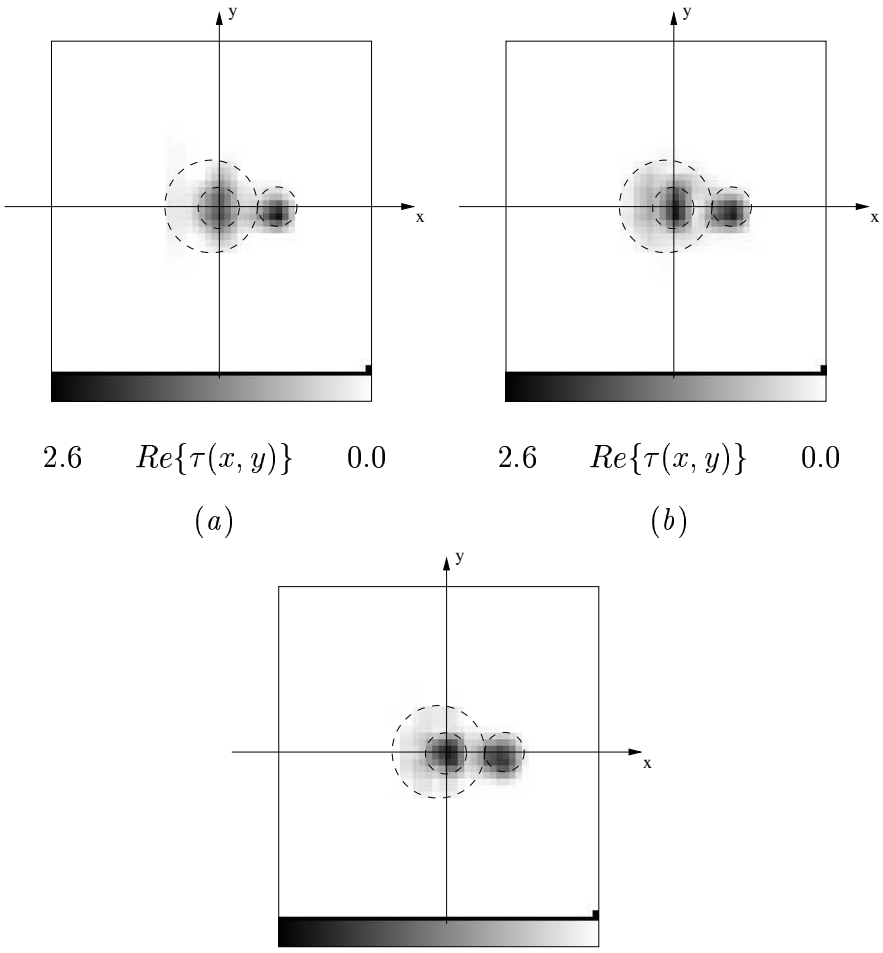

Figure 6 - M. Donelli *et al.*, "*Multi-Resolution Iterative....*"

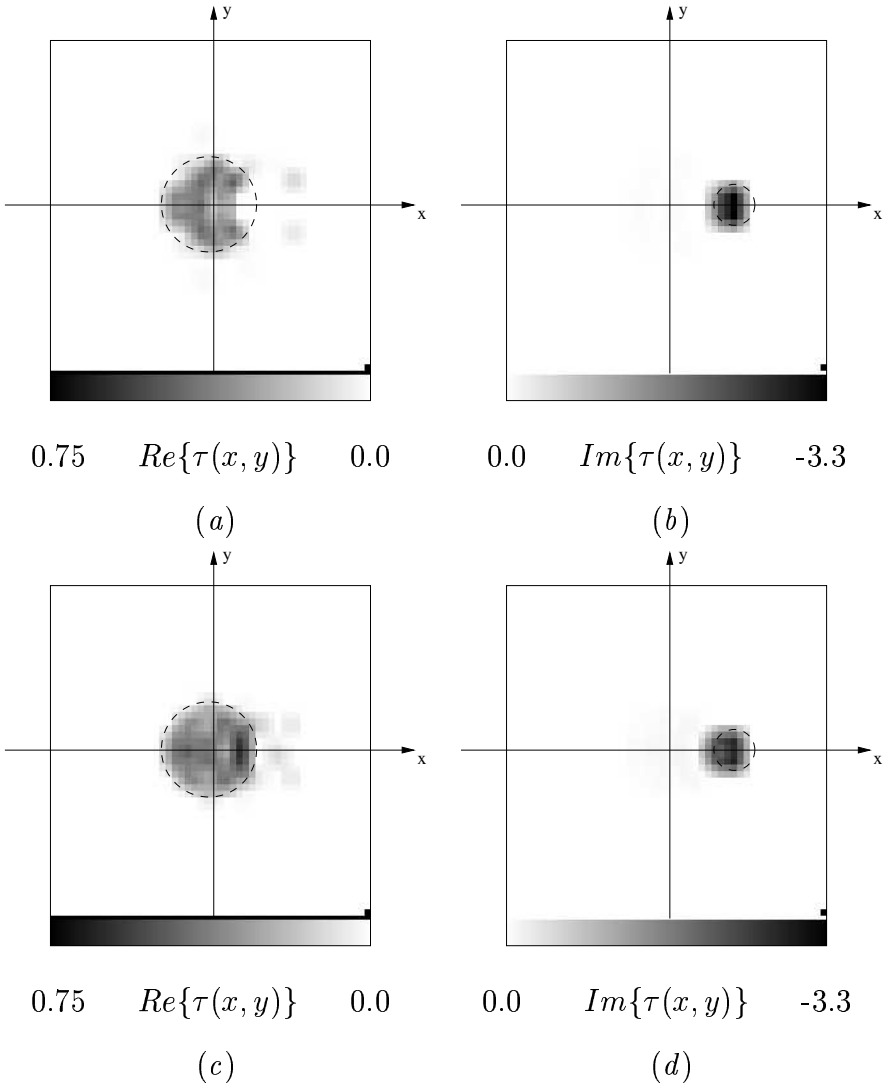

Figure 7 - M. Donelli *et al.*, "*Multi-Resolution Iterative....*"

$f \quad [GHz]$	M	V	N
2	17	8	64
3	25	8	100
4	31	8	121
5	41	8	144
6	49	8	196

Table I - M. Donelli *et al.*, "*Multi-Resolution Iterative....*"